Landau quantization effects in ultracold atom-ion collisions

Andrea Simoni and Jean-Michel Launay

Institut de Physique de Rennes, UMR 6251 CNRS-Université de Rennes 1, 35042 Rennes Cedex, France

Abstract.

We study ultracold atom-ion collisions in the presence of an external magnetic field. At low collision energy the field can drastically modify the translational motion of the ion, which follows quantized cyclotron orbits. We present a rigorous theoretical approach for the calculation of quantum scattering amplitudes in these conditions. Collisions in different magnetic field regimes, identified by the size of the cyclotron radius with respect to the range of the interaction potential, are investigated. Our results are important in cases where use of a magnetic field to control the atom-ion collision dynamics is envisioned.

1. Introduction

The central role played by the collisional interaction in determining the macroscopic properties of cold atomic gases has motivated extensive theoretical and experimental studies of neutral atom collisions at very low collision energies over the last decade. For instance, magnetic Feshbach resonances have been discovered and theoretically analyzed in several atomic species (see, *e.g.*, [1, 2]). Such resonances allow the interatomic interaction to be finely tuned, and have been used to explore a variety of phenomena such as the BEC-BCS crossover [3] and strongly correlated quantum phases [4].

While atom-ion collisions at standard temperatures are a well established subject [5], their behaviour at very low collision energy has only recently begun to raise a rapidly increasing interest. Atom-ion systems are in particular very promising candidates for the realization of collisional quantum gates [6] and for the study of ionic impurities in neutral Bose-Einstein condensates [7]. Experimental progress makes now ultracold atom-ion systems addressable in a controlled way [8]. First measurements of elastic cross sections and sympathetic cooling rates between a Bose condensed gas and a single ion held in a Paul trap have been reported in Refs. [8, 9]. Charge exchange has also been theoretically analyzed both for its interest in fundamental molecular physics and in order to quantify harmful sources of atom-loss or decoherence in the experiments [10, 11].

The presence of magnetically tuned Feshbach resonances induced by the hyperfine interaction has been demonstrated in free space in [10]. Such resonances could in principle be engineered to increase the rapidity of collisional quantum gates or to manipulate the many-body properties of a neutral gas in the presence of a charged impurity [12]. However, non trivial effects have to be taken into account to describe quantitatively atom-ion collisions in most non idealized situations, such as trap confinement [13]. An additional feature neglected in previous work [10] is the influence of the magnetic field on the translational motion of the ion, which will classically follow helicoidal rather than rectilinear trajectories. Quantum mechanically, motion in the plane transverse to the field has to be quantized, resulting in the discretization of the continuum in Landau levels [14].

The dramatic influence of even a weak magnetic field on electron photodetachment was observed a long time ago [15] and modeled using a frame transformation approximation, which relies on the much smaller length scale of the interatomic potential compared to the cyclotron radius [16]. However, the frame transformation approach cannot be applied to ultracold atom-ion collisions since the typical length scales become comparable and cannot therefore be separated already at commonly used field intensities of a few hundred Gauss (see below). Numerically exact R-matrix calculations have been carried out for hydrogen photoionization but were limited to strong magnetic fields [17]. The main goal of our paper is to develop a rigorous theory applicable to atom-ion collisions in a magnetic fields of arbitrary strength.

The paper is organized as follows. The system and general scattering properties in

a magnetic field are introduced in Sec. 2. Sec. 3 presents the numerical methods. In Sec. 4 our framework is applied to the scattering of Ca^+ ions and Na atoms. A variety of threshold, quantum interference and resonance phenomena are identified and discussed. Concluding remarks and perspectives end this work.

2. Theoretical model

2.1. Background

We consider a low energy collision between a neutral atom with a singly charged ion in the presence of a uniform static magnetic field $\vec{B}$ oriented in the z direction. We suppose that both particles have spherical symmetry, vanishing internal spin, and that the atom has an infinite mass. The latter assumption allows the number of spatial degrees of freedom to be reduced from six to three, thus avoiding complications related to the separation of the center of mass motion [18].

The spherically symmetric interparticle molecular potential $V(r)$ has a long-range behaviour determined by the second order charge induced-dipole interaction $-C_4 r^{-4}$, where $2C_4$ is the static dipolar polarizability of the neutral atom. The detailed shape of the potential well is immaterial for ultracold collisions and it can be to excellent approximation described by energy-independent quantum defects or scattering lengths [13]. For this work we take therefore a simple analytical form $V(r) = D_e\,(x^{-8} - 2x^{-4})$ with $x = r/r_e$. The potential parameters D_e and r_e are adjusted to approximately agree with the published $CaNa^+$ potentials and to reproduce the $C_4 = 81.3$ a.u. value [11]. The s-wave scattering length is currently unknown for any atom-ion system. We perform therefore some exploratory studies for different scattering lengths by adding a small correction to the bottom of the potential well to vary the value of a_s in the numerical calculations [19].

The Hamiltonian for a singly positively charged ion is

$$H = \frac{\left(\vec{p} - e\vec{A}\right)^2}{2m} + V \tag{1}$$

where $\vec{A}$ is the vector potential associated to $\vec{B}$, $\vec{p}$ the generalized momentum and $e > 0$ the ion charge. The cylindrical symmetry about the direction of the magnetic field implies conservation of the axial projection L_z of the angular momentum $\vec{L} = \vec{r} \times \vec{p}$, whose quantized values will be noted $\hbar\Lambda$. It is convenient to choose the origin of the coordinates on the neutral atom and to work in the symmetric Landau gauge, in which the vector potential has the form $\vec{A} = \frac{1}{2}\vec{B} \times \vec{r}$. With this choice, after some simple algebra the Hamiltonian takes in cylindrical coordinates $\{\rho, \varphi, z\}$ the following form

$$H = \frac{p_z^2}{2m} + \frac{p_\rho^2}{2m} + \frac{L_z^2}{2m\rho^2} + \frac{m\omega^2}{2}\rho^2 - \omega \mathrm{L}_z + V \tag{2}$$

of a particle in a diamagnetic potential of Larmor angular frequency $\omega = \frac{eB}{2m}$ interacting with a fixed center of force V. The coordinate ρ is the distance from the z axis, p_ρ is its conjugate momentum and p_z is the linear momentum in the direction of $\vec{B}$.

Conservation of the axial angular momentum reduces the orbital Zeeman term $\omega Ł_z$ to a constant but its influence on the spectrum of H is essential. In fact, quantized energies for ion motion in the plane orthogonal to $\vec{B}$, the Landau levels [14], can be expressed in terms of Λ and of the radial quantum number n by

$$E_{n\Lambda} = \hbar\omega \left(2n + |\Lambda| - \Lambda + 1\right) \quad , \quad n = 0, 1, 2, \cdots. \tag{3}$$

Eigenvalues have therefore infinite degeneracy, a quantum counterpart to the classical freedom to choose the cyclotron orbit center keeping the energy fixed. The level spacing $2\hbar\omega$ for $n \to n \pm 1$ transitions corresponds to the energy of the classical cyclotron motion with angular frequency twice the Larmor frequency of precession, $\omega_c = eB/m = 2\omega$.

The explicit expression of the eigenfunctions for planar motion with azimuthal angle φ is well known (see, e.g., Ref. [14])

$$\phi_{n\Lambda}\left(\rho, \varphi\right) = N_{n\Lambda} y^{|\Lambda|} L_n^{|\Lambda|}\left(y^2\right) e^{-y^2/2} e^{i\Lambda\varphi} \quad , \quad y = \frac{\rho}{a_{\rm ho}}, \tag{4}$$

where $a_{\rm ho} = \sqrt{\hbar/m\omega}$ is the harmonic oscillator length and $N_{n\Lambda}$ a normalization constant. The quantum description of helicoidal motion is finally completed by a uniform translation in the z direction

$$\Phi^E_{n\Lambda}\left(\vec{r}\right) = \phi_{n\Lambda}\left(\rho, \varphi\right) |k_n|^{-1/2} e^{ik_n z}. \tag{5}$$

Note that to simplify the notation we have defined $k_n = k_{n\Lambda}$ dropping the conserved quantum number Λ. Conservation of the total energy E determines the magnitude of the longitudinal wave vector

$$E = \frac{\hbar^2 k_n^2}{2m} + E_{n\Lambda}. \tag{6}$$

where the first term on the rhs is the kinetic energy in channel n, $E_{\rm kin} = \dfrac{\hbar^2 k_n^2}{2m}$.

Classically, as the atom and the ion approach, the spherically symmetric interaction distorts the cyclotron orbit modifying the energy distribution between longitudinal and transverse degrees of freedom. Quantum mechanically, a Landau collisional state $\Phi^E_{n\Lambda}$ can be either reflected or transmitted across the collision center with different probability amplitudes. In general, a collision starting with initial quantum number n will populate all states $\Phi^E_{n'\Lambda}$ energetically accessible at energy E with a transition probability amplitude $f_{n'n}$. These energetically open channels are characterized by $k^2_{n'} > 0$, see Eq. (6). The closed channels $k^2_{n'} < 0$ are not energetically allowed at large atom-ion separation but can be populated during the collision giving rise to dramatic resonance effects.

Inspection of the typical length scales in the problem shows the essential role played by Landau quantization for cold atom-ion collisions. In the ultracold regime, the range of the interaction can be defined in terms of the polarizability coefficient C_4 through $R^* = \sqrt{2mC_4\hbar^{-2}}$ [10]. The R^* parameter is proportional to the location R^*/π of the last node in the zero-energy wavefunction for infinite scattering length [19]. As such, it gives an estimate of the distance beyond which the wave function oscillates freely. The characteristic energy $E^* = \hbar^2/(2mR^{*2})$ sets the scale at which quantum effects become

Table 1. Characteristic energy and length scales as defined in the text for few sample atom-ion systems in a magnetic field $B = 500$ G. The oscillator length at this value of the field is $a_{\rm ho} = 3066 a_0$. Calculations use the reduced mass of the atom-ion dimer.

System	$R^*(a_0)$	$\hbar\omega_c(\mu\mathrm{K})$	$E^*(\mu\mathrm{K})$
$\mathrm{Na+Ca^+}$	2081	2.5	1.4
$\mathrm{Rb+Ba^+}$	4765	0.70	0.92
$\mathrm{Yb+Yb^+}$	5572	0.43	1.1

important [20]. The quantum length scale associated to cyclotron motion is $a_{\rm ho}$ which corresponds to the size of the lowest energy Landau state. The Landau levels spacing is finally given by $\hbar\omega_c$.

Let us now consider a magnetic field intensity $B = 500$ G. Tab. 1 shows the characteristic quantities for some systems of current or possible experimental interest at this value of magnetic field. One can remark that the range of the interaction is comparable to the harmonic oscillator length. Moreover, the transition between the weak $R^* \ll a_{\rm ho}$ and the strong field $R^* \gg a_{\rm ho}$ limits can be explored by varying B over an experimentally accessible range. The Landau splitting of the order of μK makes the discretized nature of the continuum in the magnetic field essential if collision energies of this order of magnitude are considered.

The scattering wavefunction presents the asymptotic $|z| \to \infty$ behaviour

$$\Psi^E_{n\Lambda}(\vec{r}) \to \Phi^E_{n\Lambda}(\vec{r}) + \sum_{k_{n'}>0} f_{n'n}\left(\mathrm{sign}(z)k_{n'} \leftarrow k_n\right) \Phi^E_{n'\Lambda}\left(\rho, \varphi, |z|\right) \tag{7}$$

in terms of an incoming $\Phi^E_{n\Lambda}$ Landau state and of scattered waves outgoing in the open channels. One should note that since the transverse motion is confined by the magnetic field, scattering is effectively one dimensional. The measurable reflection and transmission coefficients for a progressive $k_n > 0$ incoming wave can be promptly identified from Eq. (7):

$$R_{n'n} = \left|f_{n'n}\left(-k_{n'} \leftarrow k_n\right)\right|^2 \quad , \quad T_{n'n} = \left|\delta_{n'n} + f_{n'n}\left(k_{n'} \leftarrow k_n\right)\right|^2 . \tag{8}$$

A different choice of the standardization of the wavefunction for $|z| \to \infty$, the standing wave boundary conditions, will be more convenient for numerical calculations. In order to make explicit use of the invariance of the problem under the coordinate inversion $\vec{r} \to -\vec{r}$ we first define new sets of reference functions in the z motion with well defined behavior under the $z \to -z$ reflection π_z. Namely, diagonal matrices of functions $\mathbf{F}^{\pi_z}$ and $\mathbf{G}^{\pi_z}$ regular and irregular at the origin are defined for open channels and parity $\pi_z = \pm$ by

$$\begin{cases} F^+_n(z) = k_n^{-1/2}\cos(k_n z) \\ F^-_n(z) = k_n^{-1/2}\sin(k_n z) \end{cases} , \quad \begin{cases} G^+_n(z) = k_n^{-1/2}\sin(k_n|z|) \\ G^-_n(z) = -k_n^{-1/2}\mathrm{sign}(z)\cos(k_n z). \end{cases} \tag{9}$$

The corresponding reference functions for closed channels are

$$\begin{cases} F_n^+(z) = \cosh(k_n z) \\ F_n^-(z) = \sinh(k_n z) \end{cases} , \quad \begin{cases} G_n^+(z) = -\exp(-k_n|z|) \\ G_n^-(z) = -\mathrm{sign}(z)\exp(-k_n|z|). \end{cases} \tag{10}$$

With these definitions, total parity of product functions $\phi_{n\Lambda}F_n^{\pm}$ and $\phi_{n\Lambda}G_n^{\pm}$ is $p = \pi_z(-1)^{\Lambda}$. We can now define a real reactance matrix $\mathbf{K}^{\pi_z}$ for each $\pi_z = \pm$ and angular momentum Λ according to the asymptotic behaviour [21]

$$\Psi_{n\Lambda}^{Ep}(\vec{r}) \to \phi_{n\Lambda}(\rho,\varphi)\, F_n^{\pm}(z) - \sum_{n'} K_{n'n}^{\pi_z}\phi_{n'\Lambda}(\rho,\varphi)\, G_n^{\pm}(z) \quad , \quad |z| \to \infty. \tag{11}$$

If the transition matrix is also decomposed into symmetric and antisymmetric components $\mathbf{f}^{\pi_z}$,

$$f_{n'n}(\mathrm{sign}(z)k_{n'} \leftarrow k_n) = f_{n'n}^{+}(E) + \mathrm{sign}(z) f_{n'n}^{-}(E) \tag{12}$$

the matrix relations

$$\mathbf{f}^{\pi_z} = i\mathbf{K}^{\pi_z}\left(\mathbf{I} - i\mathbf{K}^{\pi_z}\right)^{-1} \tag{13}$$

obtained comparing (7) and (11) can then be used to determine the $\mathbf{f}^{\pi_z}$ in terms of $\mathbf{K}^{\pi_z}$. Finally, we will make use below of the unitary and symmetric scattering matrix, defined for the two parities as $\mathbf{S}^{\pi_z} = \left(\mathbf{I} + i\mathbf{K}^{\pi_z}\right)\left(\mathbf{I} - i\mathbf{K}^{\pi_z}\right)^{-1}$.

2.2. Wigner laws

The scattering quantities obey at low energy Wigner laws, valid when the asymptotic de Broglie wavelength is much larger than the range of the effective potential in a given channel. Following Ref. [22], a collision channel in which the collision energy tends to zero will be termed *new*. Similarly to the 3D case, in which Wigner laws depend on the angular momentum quantum number, even in the present 1D configuration it is convenient to treat separately the $\pi_z = \pm$ parity cases. An analysis along the lines of Ref. [22] gives the asymptotic behaviour,

$$f_{nn}^{+} \sim -1 + O(k_n) \quad , \quad f_{nn}^{-} \sim k_n. \tag{14}$$

implying that for vanishing collision energy at the n-th collision threshold a Landau state will be reflected with unit probability, irrespective of the value of Λ. Moreover, the odd transition matrix element becomes negligible with respect to the even component , such that particles will be scattered with equal probability $|f_{nn}^{+}|^2$ in forward and backward directions.

Inelastic processes consist in a transition to a Landau state of different transverse energy, and the corresponding scattering amplitudes obey for both parities the asymptotic law

$$f_{n'n}^{\pm} \sim \sqrt{k_n}, \tag{15}$$

if n is new. The transition probability to a newly energetically accessible channel is then vanishing at threshold both in reflection and transmission. A similar relation

$$f_{n'n}^{\pm} \sim \sqrt{k_{n'}} \tag{16}$$

holds in the case where n' is new.

The Wigner laws allows one to define for positive parity an effective coupling constant $g_{1\mathrm{D}}(k_n)$ finite at threshold ($k_n \to 0$), which embeds the details of the short range dynamics in a single parameter

$$f_{nn}^{+} = -\frac{1}{1 - i\dfrac{\hbar^2 k_n}{2m g_{1\mathrm{D}}}} \tag{17}$$

Such $g_{1\mathrm{D}}(k_n)$ can be used for instance to parametrize a 1D pseudopotential V_p, *i.e.* a zero-range interaction $V_p = g_{1\mathrm{D}}\delta(z)$ which generates the same elastic scattering amplitude as the full problem at momentum k_n. An associated one dimensional scattering length can be defined for one open channel as the limit value $a_{1\mathrm{D}} = -\lim_{k\to 0}\eta/k$, where $\eta(k)$ is the scattering phase shift extracted from the asymptotic wave function $\Psi_{00}^{E+}(\vec{r}) \propto \sin(k|z| + \eta)\phi_{00}(\rho)$ [23]. Its relation with the scattering amplitude is

$$\frac{a_{1\mathrm{D}}}{a_{\mathrm{ho}}} = -\frac{\hbar\omega a_{\mathrm{ho}}}{g_{1\mathrm{D}}}. \tag{18}$$

For a purely elastic collision $g_{1\mathrm{D}}$ is real, otherwise its non-vanishing imaginary part accounts for inelastic loss processes. Note that unlike the three-dimensional case, where $a_{3\mathrm{D}}$ is proportional to $g_{3\mathrm{D}}$, here the scattering length is inversely proportional to the coupling constant. We will restrict most of our discussions to $g_{1\mathrm{D}}$, since this is the quantity usually measured in experiments [24]. Moreover, pseudopotentials with coupling strength $g_{1\mathrm{D}}$ are often used to model two-body interactions in many-body theories. A numerically exact approach for the determination of the scattering amplitude and hence of the coupling constant is the subject of section 3.

2.3. Feshbach resonances in quasi 1D

Feshbach resonance theory is well established for three dimensional collisions. We shortly recall here its main elements in order to point out some differences with respect to the present quasi one-dimensional configuration. Let us focus for definiteness on the case of one open channel and one isolated resonance. We will consider positive parity scattering and drop the π_z parity label for notational convenience. A formal separation of background and resonant contributions to the scattering matrix can be performed following the standard Fano-Feshbach approach [25, 26]

$$S = S_{\mathrm{bg}}\frac{2(E - E_0 - \zeta_E) - i\gamma_E}{2(E - E_0 - \zeta_E) + i\gamma_E}, \tag{19}$$

where S_{bg} is the off-resonance scattering matrix, E_0 the energy location of the molecular state responsible for the resonance, ζ and γ the resonance shift and width, respectively. Near resonance the quantity E_0 typically presents a smooth linear dependence on the external parameters of the problem, the magnetic field or the potential depth in the present case.

At low momentum, according to the Wigner laws $S \sim (-1 - 2ika_{1D})$, $S_{bg} \sim (-1 - 2ika_{1D,bg})$, $\zeta_E \sim$ const and $\gamma_E \sim k$. Taking the $E \to 0$ limit, we obtain the resonantly modified a_{1D} as

$$a_{1D} = a_{1D,bg}\left(1 - \frac{\Delta}{E_0 + \zeta_0}\right), \tag{20}$$

where we have defined $\Delta = \lim_{k\to 0} \gamma_E/(2ka_{1D,bg})$. Note that on resonance ($E_0 = -\zeta_0$) the 1D scattering length diverges and according to (18) the system becomes non interacting, $g_{1D} \to 0$ and the transmission coefficient tends to one. This behaviour should be contrasted with the infinitely strong interaction obtained in three dimensions as the molecular state crosses the collision threshold. Note however that near resonance a_{1D} will cross zero, and g_{1D} will diverge, if $E_0 + \zeta_0 = \Delta$. With this remark, in the following we will refer to the divergence of the effective coupling constant as to a zero-energy resonance situation.

3. Numerical methods

We solve our problem in the framework of the time independent close coupling approach to potential scattering. In this method the full wavefunction is expanded in a suitable complete basis depending on a reduced set of coordinates. The choice of the basis function is inspired by the physics of the problem. Let us define a spherical system of coordinates $\{r, \theta, \varphi\}$ with origin on the collision center and polar axis in the z direction. We identify an "inner region" $r \leq R_0$ where the isotropic interatomic interaction initially dominates. The criterion for choosing the boundary R_0 is given below. In this internal region an expansion in spherical harmonics is used

$$\Psi^{Ep}_{n\Lambda}(\vec{r}) = {\sum_{\ell \geq |\Lambda|}}' r^{-1} f_{\ell n}(r) Y_{\ell\Lambda}(\hat{r}), \tag{21}$$

where the sum $\sum'$ runs only over even or odd values of ℓ for positive or negative parity, respectively. The coupled channel Schrödinger equation takes the form

$$\left[-\mathbf{I}\frac{\hbar^2}{2m}\frac{d^2}{dr^2} + \mathbf{v} + \mathbf{C} - \Lambda\omega\mathbf{I}\right]\mathbf{f}(r) = E\mathbf{f}(r). \tag{22}$$

The effective centrifugal potential $\mathbf{v}$ has a simple diagonal form with elements

$$v_\ell(r) = \frac{\hbar^2\ell(\ell+1)}{2mr^2} + V(r) \tag{23}$$

whereas the coupling matrix $\mathbf{C}$ is formed by the matrix elements of the transverse oscillator potential

$$C_{\ell'\ell} = \frac{m\omega^2 r^2}{2}\langle Y_{\ell'\Lambda}|\sin^2(\theta)|Y_{\ell\Lambda}\rangle. \tag{24}$$

Eq. (22) is solved up to R_0 using the Johnson-Manolopoulos propagator [27], which computes the log derivative matrix $\mathbf{Z} = \left(\frac{d}{dr}\mathbf{f}\right)\mathbf{f}^{-1}$ along a reaction coordinate using embedding propagators.

In the external $r > R_0$ region it is more natural to use cylindrical coordinates and an orthogonal basis of Landau oscillator states, Eq. (4)

$$\Psi^{Ep}_{n\Lambda}(\vec{r}) = \sum_{n'} h_{n'n}(z)\phi_{n'\Lambda}(\rho,\varphi). \tag{25}$$

The coupled channel Schrödinger equation in the cylindrical basis becomes

$$\left[-\mathbf{I}\frac{\hbar^2}{2m}\frac{d^2}{dz^2} + \mathbf{E}_L + \mathbf{u}\right]\mathbf{h}(z) = E\mathbf{h}(z). \tag{26}$$

The diagonal matrix $\mathbf{E}_L$ is composed by the Landau levels (3) and coupling $\mathbf{u}$ arises from the spherical atom-ion interaction V. In practice we will always switch to the cylindrical representation at distances where the $V(r) = -C_4 r^{-4}$ asymptotic form is accurate. Moreover, in the same region the size of transverse oscillator states is much smaller than the radial coordinate r, such that a series expansion in the small parameter $a_{\rm ho}/r$ can be performed. We find matrix elements

$$u_{n'n} = \langle\phi_{n'\Lambda}|V|\phi_{n\Lambda}\rangle = -\frac{C_4}{z^4}\left(1 - \frac{2}{z^2}\langle\phi_{n'\Lambda}|\rho^2|\phi_{n\Lambda}\rangle + \cdots\right). \tag{27}$$

The second term in the expansion is rapidly decreasing $\sim z^{-6}$ and in the present calculations we only retain lower order $\sim z^{-4}$ diagonal coupling elements u_{nn} for both open and closed channels.

The representations (21) and (25) are matched on the spherical surface S_0 defined by $r = R_0$. We find that to insure optimal numerical convergence one should choose R_0 in such a way that the relevant Landau states are localized in the two hemispheres without significant overlap on the equatorial plane ‡. The matching procedure is analogous to the one used in reactive scattering [28, 29]. We anticipate that the change from spherical to cylindrical geometry is at the origin of the peculiar scattering and resonance phenomena described in the next section.

In the external region $r > R_0$ we integrate inward the equations (26) from very large values of z, with starting value the asymptotic boundary condition (9)-(10). Let us denote the corresponding matrix solutions $\hat{\mathbf{F}}^{\pm}$ and $\hat{\mathbf{G}}^{\pm}$, which retain diagonal form due to the neglect of the off diagonal elements in the coupling $\mathbf{u}$. The scattering solution is represented as

$$\Psi^{Ep}_{n\Lambda}(\vec{r}) = \sum_{n'}\left[\hat{F}^{\pm}_{n'}(z)\delta_{n'n} - \hat{G}^{\pm}_{n'}(z)K^{\pi_z}_{n'n}\right]\phi_{n'\Lambda}(\rho,\varphi) \quad , \quad r > R_0. \tag{28}$$

Continuity of the scattering wavefunction and of its normal derivative on the spherical surface S_0 is used to determine $\mathbf{K}$ in terms of the logarithmic derivative matrix $\mathbf{Z}$. The projection matrices

$$\begin{aligned}\mathcal{F}_{\ell n} &= \langle Y_{\ell\Lambda}|\hat{F}_n\phi_{n\Lambda}\rangle_{S_0}\\ \mathcal{F}'_{\ell n} &= \langle Y_{\ell\Lambda}|\frac{\partial}{\partial r}(\hat{F}_n\phi_{n\Lambda})\rangle_{S_0}\end{aligned} \tag{29}$$

‡ Typically, $R_0 = 10a_{\rm ho}$ insures a good convergence for collisions starting in the lowest Landau levels.

needed to this aim [29] are numerically evaluated using Gauss-Legendre quadratures. Similar projection matrices $\mathcal{G}_{\ell n}$ and $\mathcal{G}'_{\ell n}$ involving the irregular reference functions are defined by replacing $\hat{F}$ with $\hat{G}$ on the rhs of (29). The reactance matrix is finally obtained for each parity using the equation [29]

$$\mathbf{K} = \left(\mathbf{Z}\mathcal{G} - \mathcal{G}'\right)^{-1} \left(\mathbf{Z}\mathcal{F} - \mathcal{F}'\right). \tag{30}$$

4. Results and discussion

In this section we apply our formalism to atom-ion diffusion with $\Lambda = 0$, a somewhat idealized situation to test our theoretical formalism which can however be in principle experimentally realized. For instance, instantaneous switching of a magnetic field in the propagation direction of an ion beam would project the plane wave describing the beam on a superposition of Landau states with different n and $\Lambda = 0$ without affecting the longitudinal momentum k. A successive measurement of the transverse energy could be used to select the desired initial asymptotic state n for the collision.

The default molecular parameters we choose for our model correspond to the Na+Ca^+ system. However, previous work has shown that the short range molecular physics can be accurately described in the ultracold regime by a single quantum defect parameter independent of energy and angular momentum, which can be identified with the s-wave three-dimensional scattering length a_s [10]. Within this approximation, our results will be cast in an essentially system independent form by presenting them in terms of the only independent dimensionless groups

$$\frac{a_s}{R^*} \quad , \quad \frac{E}{\hbar\omega_c} \quad , \quad \frac{a_{\rm ho}}{R^*}, \tag{31}$$

that can be built using the physical parameters of the problem. Note that in this work we set m equal to the reduced mass of the system, for future comparison with the free-space results [10].

We first consider collisions starting in the lowest Landau level $n = 0$ at zero collision energy and calculate the effective coupling constant $g_{\rm 1D}(k_0 \to 0)$. We make the three dimensional scattering length a_s vary from infinite negative to positive infinite values by artificially modifying the interaction potential. The variation of a_s in units of $a_{\rm ho}$ will be mapped to a finite interval by introducing the normalized quantum defect $\xi = (2/\pi)\arctan(a_s/a_{\rm ho})$. This analysis will be repeated for three values of $a_{\rm ho}$. We will then analyze the behaviour with the collision energy of the scattering observables for some selected values of $a_{\rm ho}$ and a_s.

4.1. Weak field regime

Let us first fix a value of B such that the size of the lowest Landau state is significantly larger than the interaction range. We will refer to this condition as the weak field limit, and choose more specifically $a_{\rm ho} = 10R^*$ ($B = 10.9$ G). A salient feature observed in Fig. 1 is the strong divergence of the effective coupling constant at a characteristic

value of a_s. That is, the effective 1D coupling strength can be tuned to virtually any value by modifying the value of a_s with respect to $a_{\rm ho}$, for instance through a variation of the applied magnetic field. We stress that this zero energy resonance arises from the quantization of the continuum in Landau levels and does not depend on resonance phenomena preexisting in free space. As such it can be termed a geometric resonance effect.

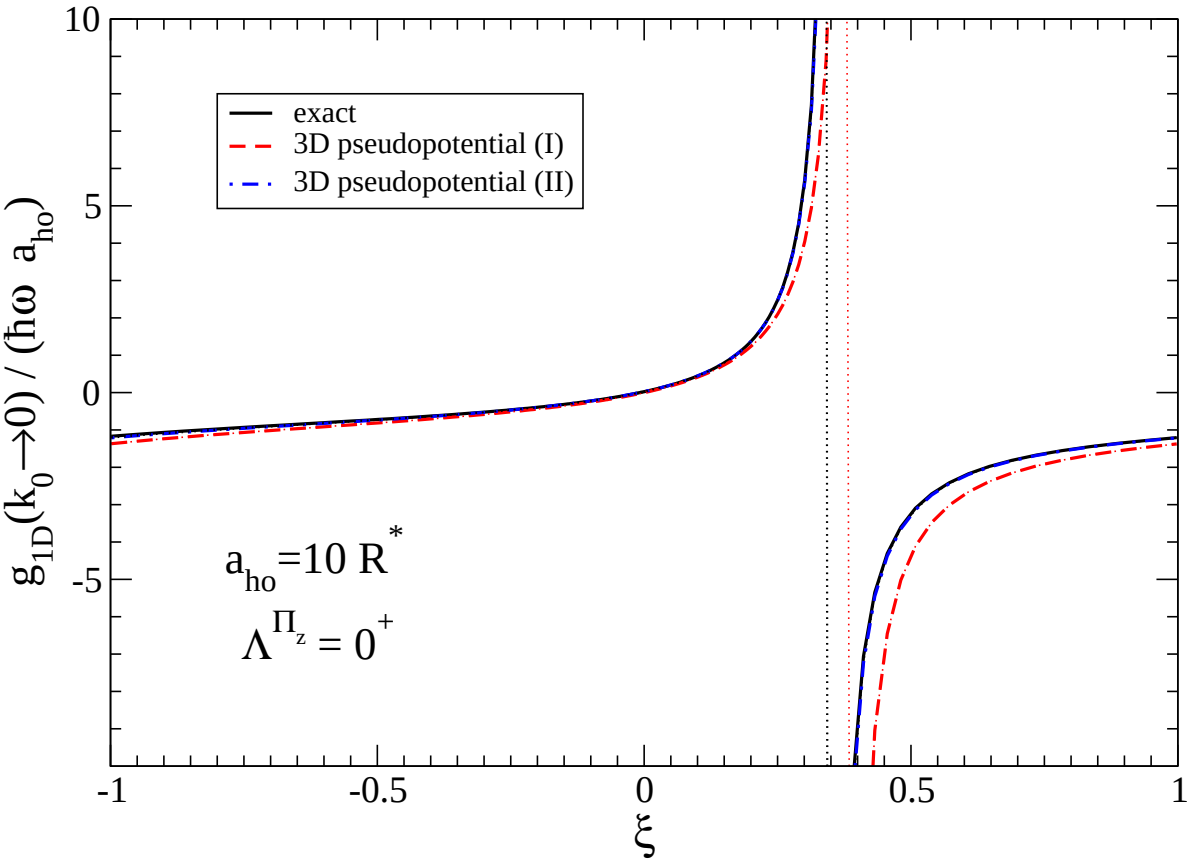

Figure 1. Numerically computed effective coupling constant for Ca^++Na collisions in a weak magnetic field with $a_{\rm ho} = 10R^*$ as a function of the normalized scattering phase $\xi = (2/\pi)\arctan(a_s/a_{\rm ho})$ for axial angular momentum $\Lambda^{\pi_z} = 0^+$ (full line). Vertical dotted lines denote the position where g_{1D} diverges ($a_{1D} = 0$). Energy independent end energy dependent pseudopotential approximations (see text) labeled I and II respectively are also shown.

Interestingly, since in the weak field limit the range of the potential can be neglected with respect to the transverse extension of the Landau state, the interaction V can be expected to be well described by a zero range 3D pseudopotential. With this approximation, Eq. (26) for $\Lambda = 0$ reduces to an analytically solvable model [23, 30]. The effective coupling constant of Ref. [23] is

$$\frac{g_{1D}}{\hbar\omega a_{\rm ho}} = 2\frac{a_s}{a_{\rm ho}}\left(1 + \frac{a_s}{a_{\rm ho}}\zeta(1/2)\right)^{-1}, \tag{32}$$

where ζ is the Riemann zeta function and $\zeta(1/2) = -1.46035$. The zero-order result

$g_{1D} = 2a_s\hbar\omega$, obtained by neglecting the second term in the parenthesis on the rhs, simply represents the renormalization of a_s obtained in the Born approximation by averaging the three-dimensional pseudopotential over the initial transverse Landau state. However, Eq. (32) also shows that a confinement-induced resonance arising from virtual excitations to asymptotically closed Landau states should appear for $a_s = -a_{\rm ho}/\zeta(1/2) \simeq 0.6848\ a_{\rm ho}$.

This nontrivial prediction is confirmed by the comparison with our numerical calculation shown in Fig. 1. The small shift in the resonance position can be understood by realizing that the result (32) is exact only in the limit of vanishingly small *axial* collision energy. However, when the atom and the ion are close together the relative energy E in their unconfined 3D motion does not vanish but is rather equal to the zero point energy $\hbar\omega$, see Eq. (3). This correction can be introduced by using an energy dependent 3D peudopotential [31], which replaces the zero energy parameter a_s with its finite energy counterpart $-\tan(\delta_{3D})/k_{3D}$. Here δ_{3D} is the s-wave phase shift at energy E and $k_{3D} = \sqrt{2mE/\hbar^2}$ is the wave vector in the three-dimensional motion. With this modification our numerical calculation becomes virtually identical to Eq. (32) thus confirming the accuracy of the pseudopotential approximation even for a long-range r^{-4} potential under the appropriate conditions.

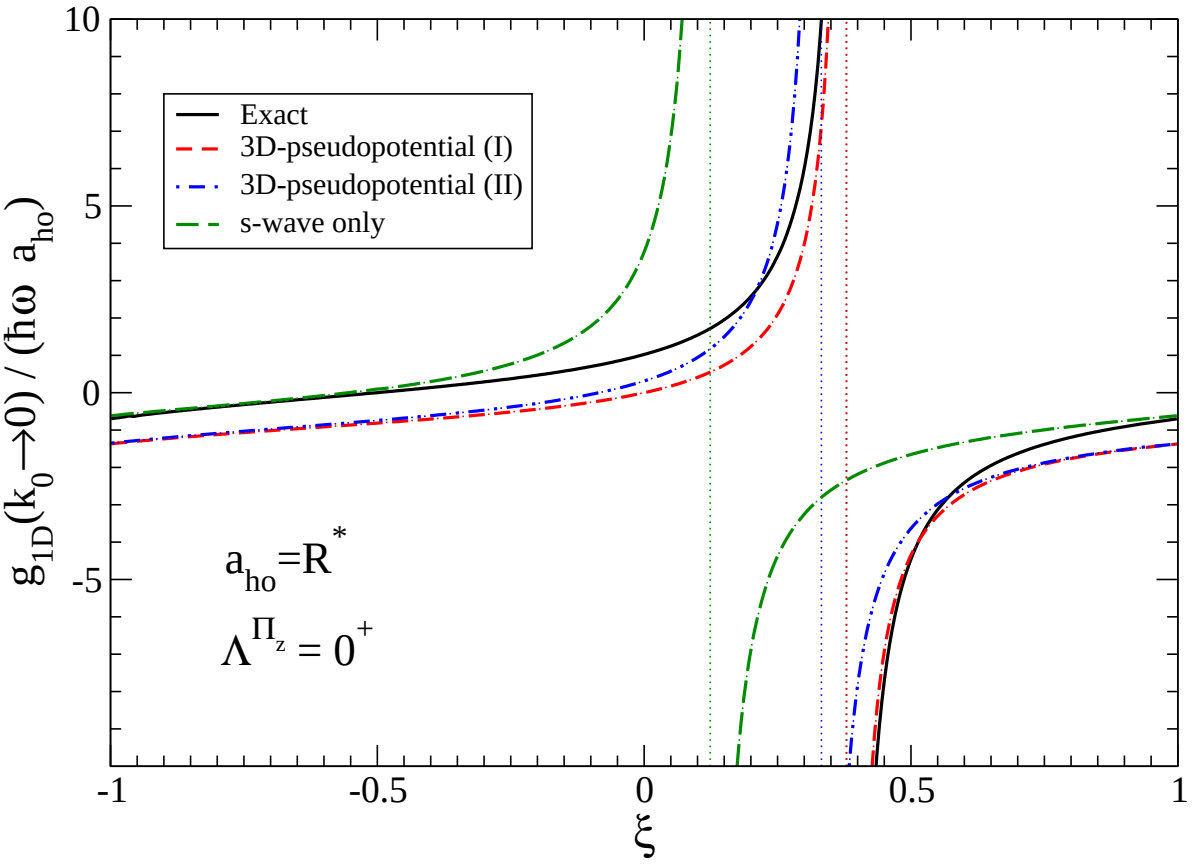

Figure 2. Same as figure 1 but in the intermediate field case $a_{\rm ho} = R^*$. The result of a purely s-wave calculation with the full molecular potential is also shown (see text) .

Since the zero point energy is small with respect to the centrifugal barriers in Eq. (22) one can expect, as indeed proven by the agreement with the s wave model (32), that diffusion in partial waves $\ell > 0$ should be significantly suppressed. Our numerical approach allows us to check this property by a direct calculation. To this aim, we set $V = 0$ in the $v_{\ell>0}$ components of the interaction matrix $\mathbf{v}$. The non s-wave potentials are also turned off in the external region by using in the projection matrix elements (29) with $\ell > 0$ the unperturbed waves F and G in the place of $\hat{F}$ and $\hat{G}$. Note that in spite of the fact that dynamically a single partial wave contributes to scattering, one cannot simply use a unique $\ell = 0$ in the expansion (21), since a sufficient number of partial waves is in any instance cinematically necessary in order to represent the relevant Landau states on the spherical surface S_0 of radius R_0. The result of this purely s-wave calculation is not included in Fig. 1 as it is virtually indistinguishable from the exact result.

4.2. Intermediate field regime

Let us now consider the variation of $g_{1\mathrm{D}}$ with a_s in the intermediate field regime $a_{\mathrm{ho}} = R^*$ ($B = 1.09\times10^3$ G). Like in weak field conditions, a single geometric resonance is observed in the numerical simulation, see Fig. 2. The pseudopotential result in Eq. (32) in the energy-independent (I) and energy-dependent (II) formulations is only qualitatively correct. The purely s-wave calculation shows a significant shift in the resonance position from both the exact calculation and the pseudopotential models.

These findings can be rationalized as follows. The discrepancy between the pseudopotential and the purely s-wave result demonstrates the breakdown of the assumption of a zero-range potential, that is the importance of the long-range interplay between atom-ion and magnetic field potentials. The disagreement between the s-wave and the exact result is due to the important contribution of higher order partial waves. This contribution does not vanish even in the $k \to 0$ limit because of the zero point energy. Its value ($\simeq 3\mu$K), a factor 10^2 larger than in the weak field case, and the long range nature of the potential insure that a few partial waves are scattered from the potential. More quantitatively, by artificially varying the number of partial waves as described above we find that a calculation restricted to $\ell = 0 - 4$ determines with high accuracy $g_{1\mathrm{D}}$. The good agreement in the resonance position between the exact result and the pseudopotential (I) approximation should be regarded as merely coincidential, stemming from the compensation of long-range and higher order partial waves effects.

4.3. Strong field regime

Finally, Fig. 3 shows the behaviour of $g_{1\mathrm{D}}$ for a strong field case $a_{\mathrm{ho}} = 0.1R^*$, a tight confinement condition in which the potential range is larger than the Landau orbit radius. The required magnetic field intensity is of $B = 1.09 \times 10^5$ G, a large yet experimentally attainable value. In this conditions both the pseudopotential and the purely s-wave model completely fail to reproduce the numerical results. Several zero-

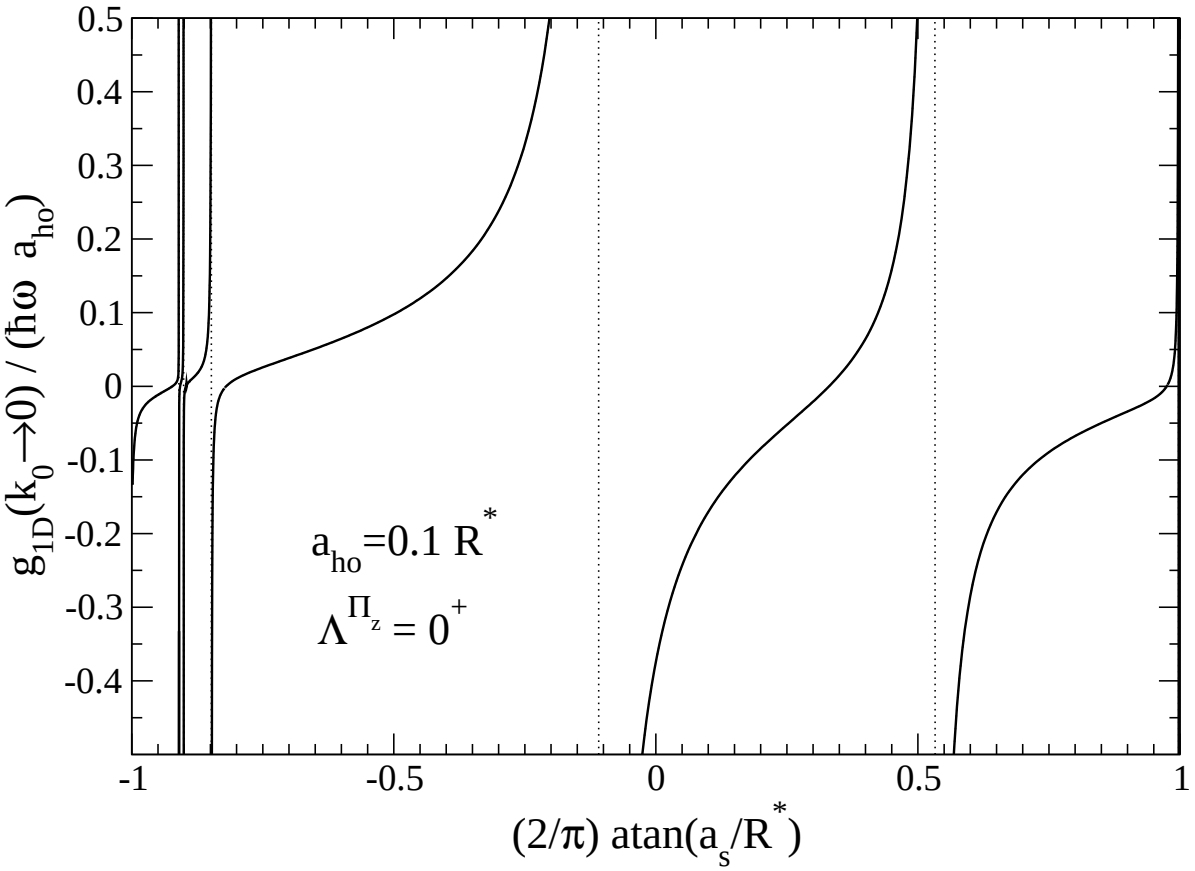

Figure 3. Same as figure 1 but in the strong field case $a_{\rm ho} = 0.1R^*$. The pseudopotential approximation breaks down in this situation and is not shown. Note that for graphical purposes the normalized quantum defect on the horizontal axis is defined in terms of R^* rather than of $a_{\rm ho}$.

energy resonances are now available as a_s (or B) is made to vary. The nature of such resonances can be understood from test calculations in which the atom-ion potential is suppressed in selected partial waves. Such calculations show that each broad feature in the $g_{1\rm D}$ of Fig. 3 arises from the combined effect of a relatively large number of partial waves $\ell = 0 - 12$. That is, due to the relatively large zero point energy ($\hbar\omega \simeq 300\mu$K) the wave function picks up a significant phase shift at short range from different partial wave effective potentials. The narrowest features observed near $\xi = -1$ can in contrast be assigned to a single or few $\ell \geq 4$ angular momentum values, suggesting that most of the amplitude of the resonant bound state is localized in the potential well region. An analysis of the bound states of the systems will be needed to assign more precisely the features observed in the present scattering calculations.

4.4. Behaviour with collision energy

The zero energy resonances described so far may shift as a function of the potential strength a_s into the scattering continuum giving rise to possible resonance effects

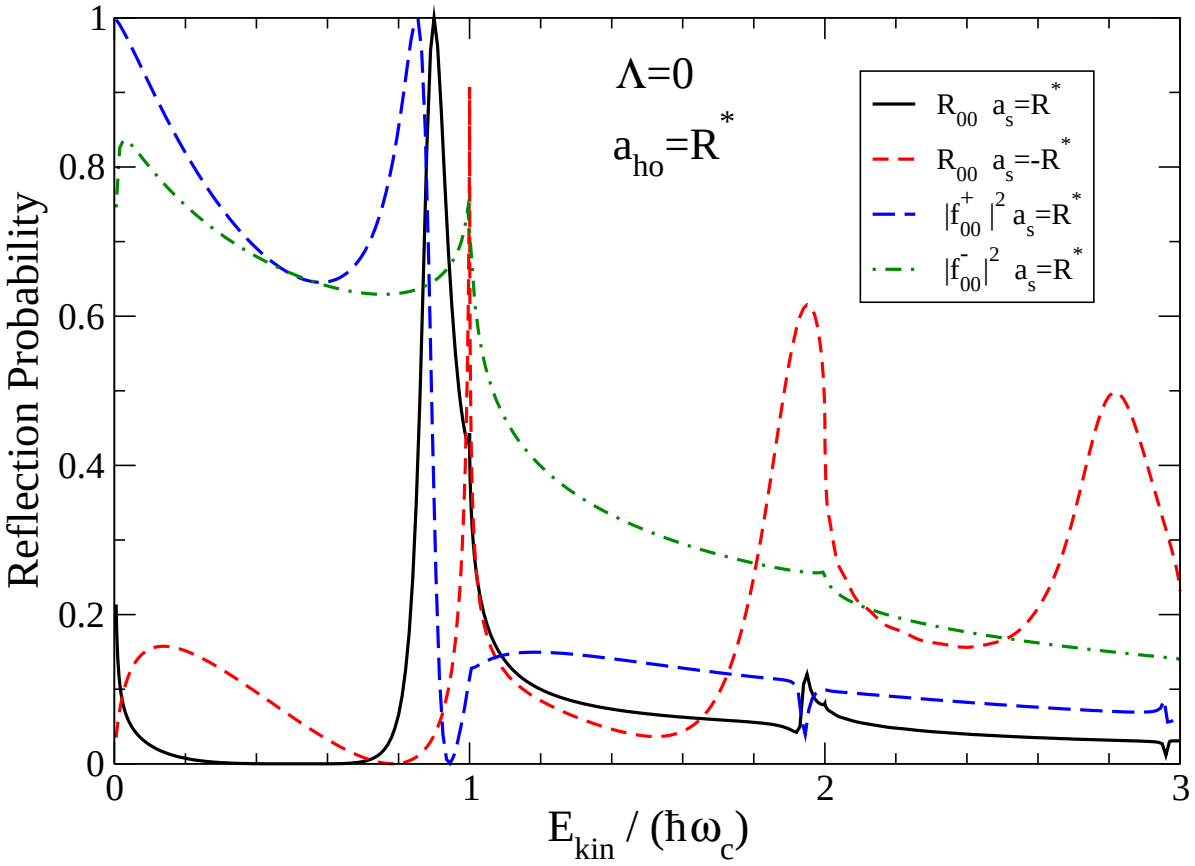

Figure 4. Elastic reflection probability for an ion in the lowest Landau level as a function of collision energy in the intermediate field case $a_{\rm ho} = R^*$. Axial angular momentum is $\Lambda = 0$ and typical values of the tridimensional scattering length $a_s = \pm R^*$ are selected. Odd and even contributions to the reflection probability are separately shown for the $a_s = R^*$ case. Resonance and threshold phenomena in the reflection probability are discussed in the text.

observable as a function of collision energy. Let us consider in detail two potentials supporting "typical" scattering lengths $a_s = \pm R^*$ in the intermediate field case $a_{\rm ho} = R^*$. Fig. 4 shows the *elastic* reflection probability R_{00} for a scattering event starting with the ion in the lowest Landau state ϕ_{00}, as a function of collision energy. A decomposition of the scattering amplitude in even and odd components shows that the small value of the reflection coefficient $R_{00} = |f_{00}^+ - f_{00}^-|^2$ between the $n = 0$ and 1 thresholds is due to interference of parity amplitudes of relatively large magnitude, see Fig. 4. A similar situation has been reported for neutral atom scattering from short-range potentials in [32]. Fig. 5 stresses the fact that the Wigner regime near the $n = 0$ threshold at which $R_{00} \to 1$ is correctly reproduced by the numerical calculation but is extremely narrow, for $a_s = -R^*$ in particular.

For $a_s = R^*$ a first peak at which R_{00} reaches one is observed below the opening of the $n = 1$ level with energy $\hbar\omega_c$. This feature arises from the positive parity part $\mathbf{f}^+$ of the scattering amplitude, and can be supposed to be a resonance arising from trapping

of the ion in a long-lived superposition of excited Landau states.

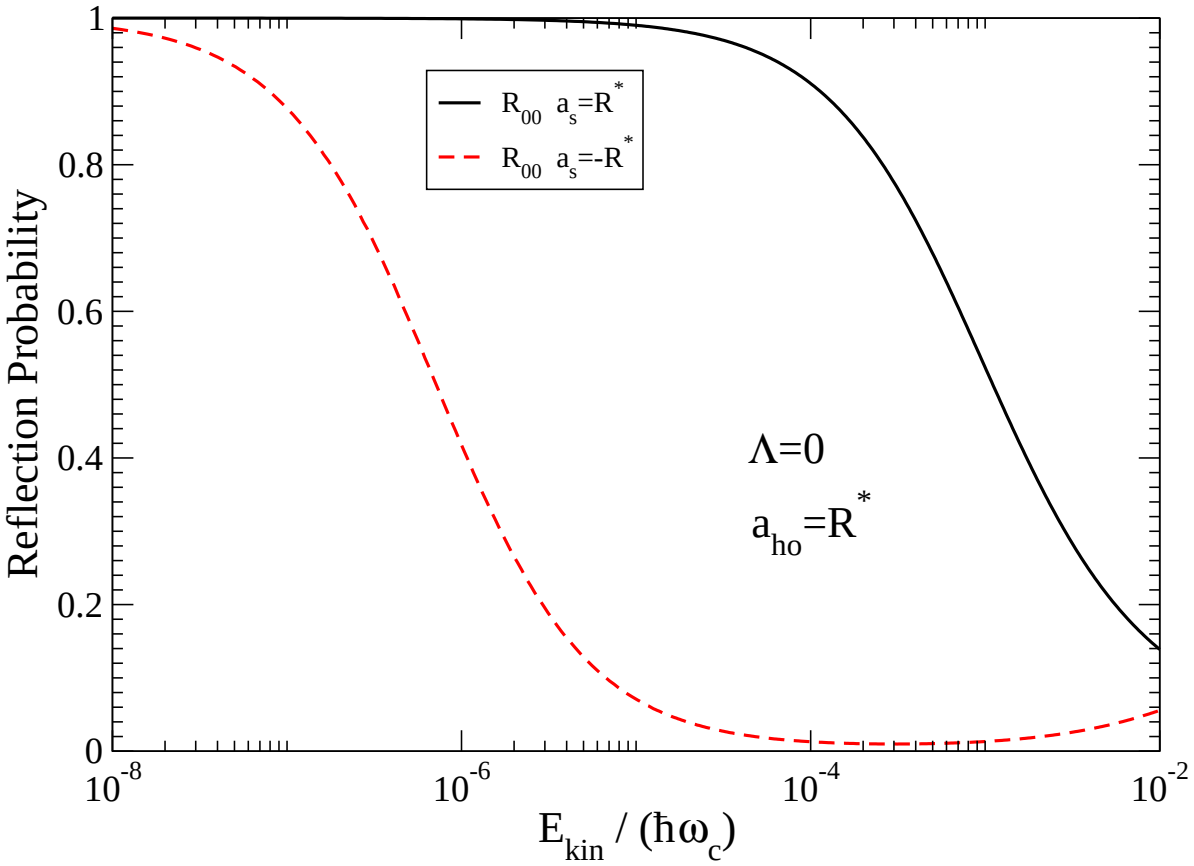

Figure 5. Near threshold elastic reflection probability for $a_s = \pm R^*$. Systems parameters are as in Fig. 4.

To confirm the resonant character of this feature we calculate the time delay matrix introduced by Smith [33], defined for each parity as

$$\mathbf{Q}^{\pi_z} = i\hbar \left(\mathbf{S}^{\pi_z}\right)^\dagger \frac{d\mathbf{S}^{\pi_z}}{dE}. \tag{33}$$

Note that $\mathbf{Q}$ is expressed in terms of the open channel scattering matrix, such that its dimension equals the number of energetically accessible channels. The evolution with energy of the largest eigenvalue q of the lifetime matrix can provide in particular information on the lifetime of the complex formed during a collision. For instance, a narrow isolated resonance far from a collision threshold is characterized by a time delay following a familiar Lorentzian profile [33, 34]. In general, at very low collision energy threshold effects produce deviations from this simple picture making the analysis less direct [35]. In the present case the situation is simpler, since the lifetime obtained from $\mathbf{Q}^+$ shows a pronounced bell shape profile of width much smaller than its central energy.

This analysis provides conclusive evidence of the resonant nature of the feature observed in the reflection probability (see Fig. 6) and allows us to assign positive parity to the associated metastable state. As already noted in [35] the time delay diverges

positively or negatively at zero energy with a $2ma_{1D}/(\hbar k)$ law, corresponding to the classical time to span the $2a_{1D}$ distance.

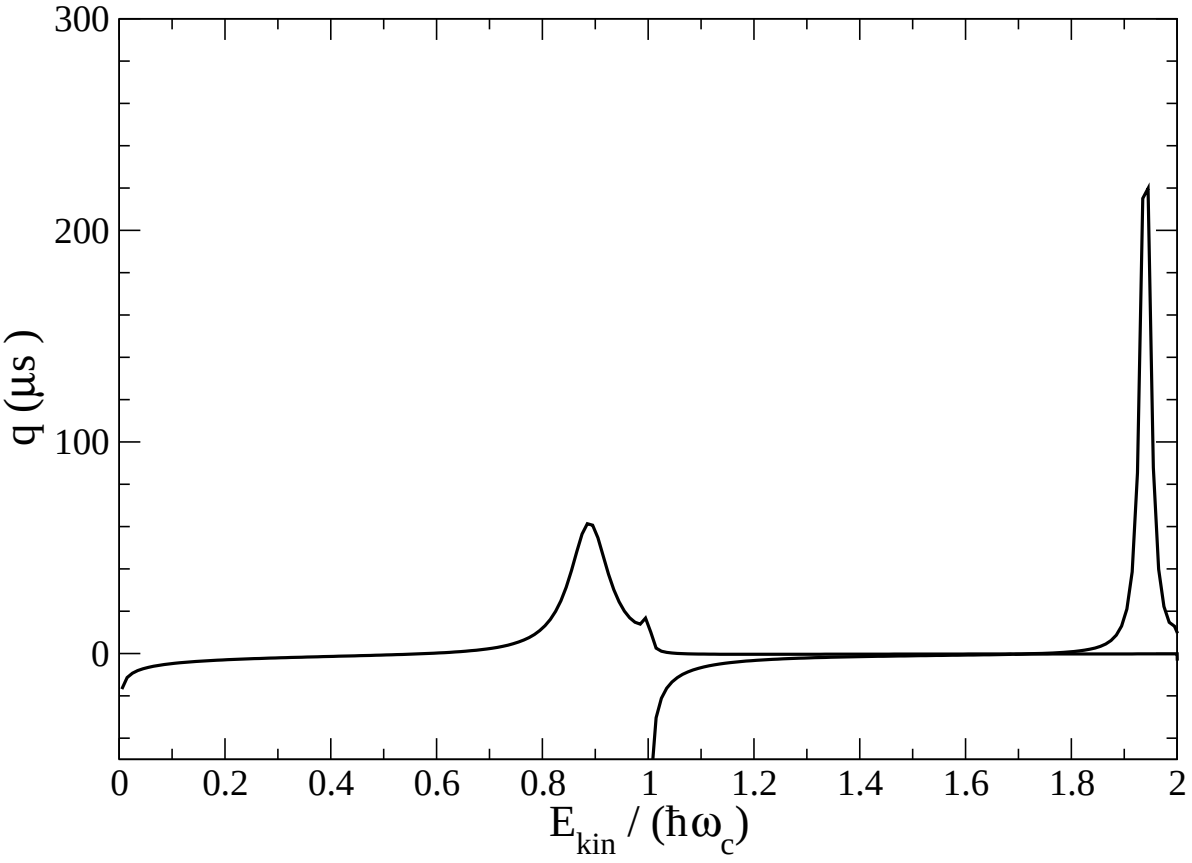

Figure 6. The two largest eigenvalues of the time delay matrix as a function of collision energy for the $a_s = R^*$ collision in the intermediate field case of Fig. 4. Only $\pi_z = +$ eigenvalues are shown. The long-lived isolated peaks are conclusively of resonant origin.

Below the second $n = 1$ and third $n = 2$ thresholds additional rapid variations with energy of smaller amplitude appear in R_{00}. Again, the time delay analysis shown in Fig. 6 conclusively confirms the resonant nature of these features. The dispersive-like shape observed in the reflection probability arises from interference with background scattering, whereas the small modulation amplitude is explained by quenching due to $n = 0 \to n' > 0$ inelastic processes.

Quite strikingly, such resonances seem to occur at similar locations with respect to each threshold. This property can be qualitatively interpreted using the pseudopotential analytical method of Ref. [36]. In this approach the resonance below the first threshold is assigned to a molecular state generated by the zero-range interaction in the $n > 0$ subspace of closed channels. By a straightforward generalization consisting in replacing the shift operator $A^\dagger = \sum_n |\phi_{n+1,0}\rangle\langle\phi_{n,0}|$ below Eq. (10) of [36] by $A^\dagger = \sum_n |\phi_{n+m,0}\rangle\langle\phi_{n,0}|$, one can show that if a resonant state is present below the $n = 1$ level there has to be a corresponding one below the mth threshold. Similar

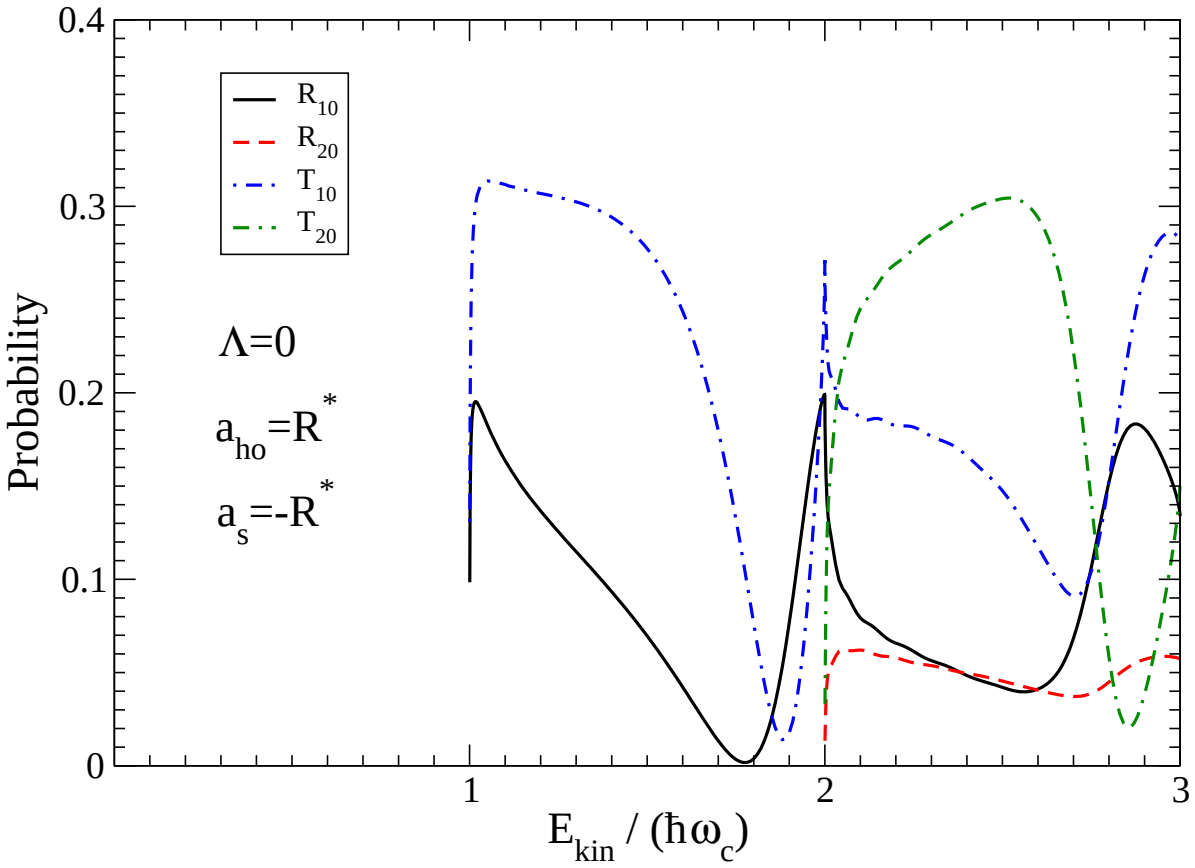

Figure 7. Inelastic reflection and transmission probability for an ion in the lowest Landau level as a function of collision energy in the intermediate field case $a_{\rm ho} = R^*$ for $\Lambda = 0$ and $a_s = -R^*$.

regularities in the Landau resonance spectrum have also been proved in low-energy electron photodetachment using a simplified model which assumes resonant states confined in the $z = 0$ plane [37].

The $a_s = -R^*$ reflection coefficient shows an evident cusp at the opening of the first threshold. Near the higher thresholds, rounded step features are also evident. These features arise from the non analyticity of the scattering amplitude near the opening of a new threshold and do not have resonant origin. In fact, as shown by Newton both sharp and rounded features can appear at threshold openings [38].

We also show in Fig. 7 inelastic transition probabilities from the lowest to excited Landau states for $a_s = -R^*$. Note that T_{n0} and R_{n0} vanish at the nth threshold, in agreement with the Wigner laws, and are otherwise of significant magnitude. The T_{n0} and R_{n0} differ in general, showing once again that scattering from odd partial waves is non negligible in the intermediate field case, and introduces a significant forward-backward asymmetry. As expected the R_{n0} and T_{n0} do not vanish at thresholds $m \neq n$, but present cusps and rounded step singularities similar to the one observed in the elastic probabilities.

Finally, we compute the elastic reflection probability in the strong field limit

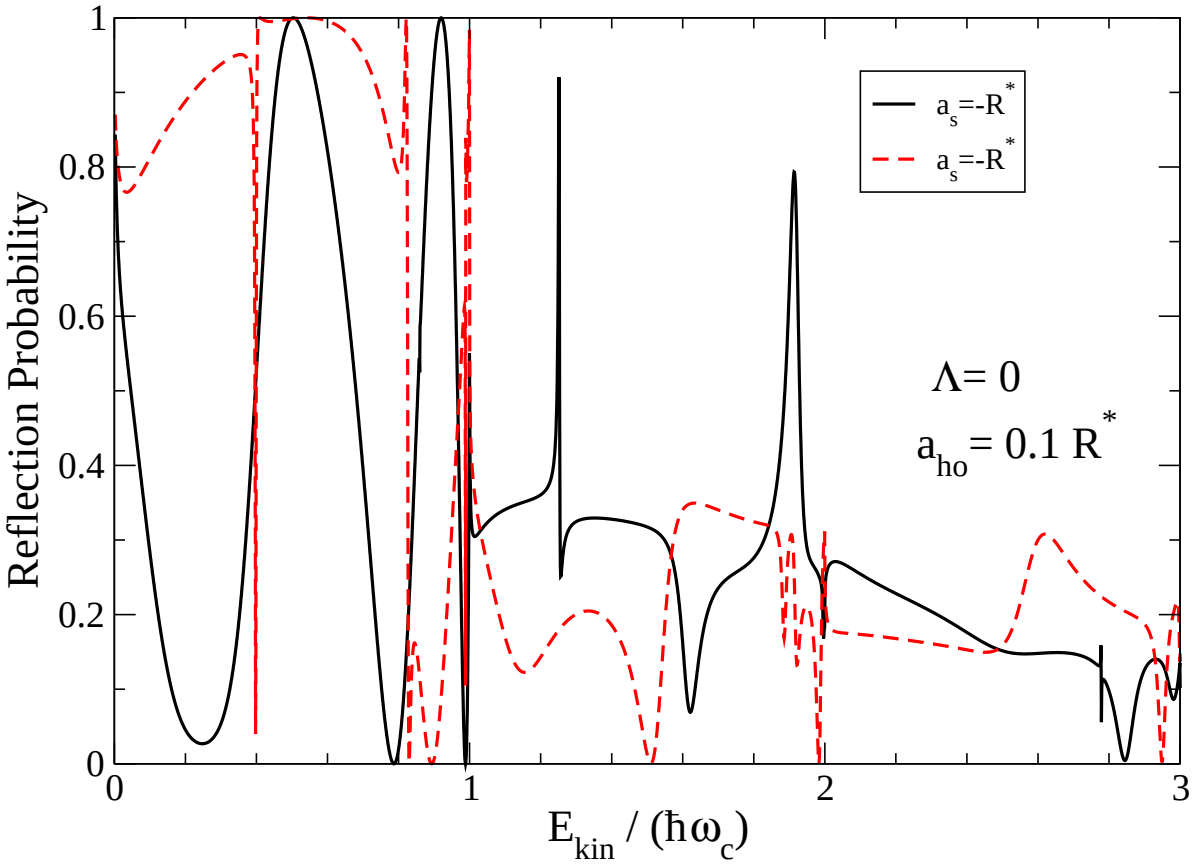

Figure 8. Elastic reflection probability for an ion in the lowest Landau state as a function of collision energy in the strong field case $a_{\rm ho} = 0.1R^*$. Axial angular momentum is $\Lambda = 0$ and typical values of the tridimensional scattering length $a_s = \pm R^*$ are selected.

(Fig. 8). The rich resonance structure characteristic of zero energy scattering has a finite energy counterpart. In fact, multiple resonance peaks are now observed between Landau thresholds. The narrowest features are most likely associated to bound states of relatively large ℓ components. At variance with the intermediate-field case, a decomposition of the transition matrix identifies the resonance peaks as originating from both positive and negative parities. Cusp and rounded steps stemming from the non analytical behaviour of the scattering matrix and from interference effects between parity components of the scattering amplitude are also visible near the opening of new energy thresholds.

5. Conclusions and outlook

In conclusion, we have presented a rigorous computational approach to study atom-ion collisions in the presence of a magnetic field. The weak-field case maps to a well understood analytical model. In contrast, we have shown that a novel regime of strong confinement can be reached in atom-ion systems at experimentally attainable values

of the magnetic field. A series of zero- and finite-energy resonances associated to high order partial waves appears in this case. The resonance phenomena we have analyzed in this work should play an important role in applications based on magnetic control of the atom-ion dynamics.

In a forthcoming paper we will present our results for the qualitatively different case of $|\Lambda| > 0$ collisions and consider the case of a scattering center not necessarily placed on the axis of the cyclotron orbit. In perspective, it will be interesting to investigate the interplay of pre-existing atom-ion magnetic Feshbach resonances and of Landau quantization. Moreover, in cases where the atom cannot be treated as infinitely massive, quasi separability of the center of mass motion might give rise to still unexplored resonance phenomena.

6. Acknowledgments

A. S. gratefully acknowledges support from CNRS and Rennes-Metropole.

7. References

[1] H. Wang, A. N. Nikolov, J. R. Ensher, P. L. Gould, E. E. Eyler, W. C. Stwalley, J. P. Burke, J. L. Bohn, Chris. H. Greene, E. Tiesinga, C. J. Williams, and P. S. Julienne. Ground-state scattering lengths for potassium isotopes determined by double-resonance photoassociative spectroscopy of ultracold ^{39}K. *Phys. Rev. A*, 62:052704–1–4, 2000.

[2] A. Simoni, M. Zaccanti, C. D'Errico, M. Fattori, G. Roati, M. Inguscio, and G. Modugno. Near-threshold model for ultracold KRb dimers from interisotope Feshbach spectroscopy. *Phys. Rev. A*, 77:052705–1–8, 2008.

[3] C. A. Regal, M. Greiner, and D. S. Jin. Observation of resonance condensation of fermionic atom pairs. *Phys. Rev. Lett.*, 92:040403–1–4, 2004.

[4] T. Volz, N. Syassen, D. M. Bauer, E. Hansis, S. Dürr, and G. Rempe. Preparation of a quantum state with one molecule at each site of an optical lattice. *Nature Physics*, 2:692–695, 2006.

[5] J. B. Delos. Theory of electronic transitions in slow atomic collisions. *Rev. Mod. Phys*, 53:287–357, 1981.

[6] H. Doerk, Z. Idziaszek, and T. Calarco. Atom-ion quantum gate. *Phys. Rev. A*, 81:012708–1–13, 2010.

[7] R. Côté, V. Kharchenko, and M. D. Lukin. Mesoscopic molecular ions in Bose-Einstein condensates. *Phys. Rev. Lett.*, 89:093001–1–4, 2002.

[8] C. Zipkes, S. Palzer, C. Sias, and M. Köhl. A trapped single ion inside a Bose-Einstein condensate. *Nature*, 464:388–391, 2010.

[9] A. T. Grier, M. Cetina, F. Oručević, and V. Vuletić. Observation of cold collisions between trapped ions and trapped atoms. *Phys. Rev. Lett.*, 102:223201–1–4, 2009.

[10] Z. Idziaszek, T. Calarco, P. S. Julienne, and A. Simoni. Quantum theory of ultracold atom-ion collisions. *Phys. Rev. A*, 79:010702(R)–1–4, 2009.

[11] O. P. Makarov, R. Côté, H. Michels, and W. W. Smith. Radiative charge-transfer lifetime of the excited state of $(\mathrm{naca})^+$. *Phys. Rev. A*, 67:042705–1–5, 2003.

[12] J. Goold, H. Doerk, Z. Idziaszek, T. Calarco, and Th. Busch. Ion-induced density bubble in a strongly correlated one-dimensional gas. *Phys. Rev. A*, 81:041601(R)–1–4, 2010.

[13] Z. Idziaszek, T. Calarco, and P. Zoller. Controlled collisions of a single atom and an ion guided by movable trapping potentials. *Phys. Rev. A*, 76:033409–1–16, 2007.

[14] L. D. Landau and E. M. Lifschitz. Quantum mechanics. *(Butterworth-Heinemann, Oxford)*, 1999.

[15] W. A. M. Blumberg, R. M. Jopson, and D. J. Larson. Precision laser photodetachment spectroscopy in magnetic fields. *Phys. Rev. Lett.*, 40:1320–1323, 1978.

[16] C-H. Greene. Negative-ion photodetachment in a weak magnetic field. *Phys. Rev. A*, 36:4236–4244, 1987.

[17] Q. Wang and C. H. Greene. r-matrix calculation of atomic hydrogen photoionization in a strong magnetic field. *Phys. Rev. A*, 44:7448–7458, 1991.

[18] J. E. Avron, I. W. Herbst, and B. Simon. Separation of center of mass in homogeneous magnetic fields. *Ann. Phys.*, 114:431–451, 1977.

[19] E. Tiesinga, C. J. Williams, P. S. Julienne, K. M. Jones, P. D. Lett, and W. D. Phillips. A spectroscopic determination of scattering lengths for sodium atom collisions. *J. Res. Natl. Inst. Stand. Tech.*, 101:505–520, 1996.

[20] P. S. Julienne and F. H. Mies. Collisions of ultracold trapped atoms. *J. Opt. Soc. Am. B*, 6:2257–2269, 1989.

[21] M. L. Goldberger and K. M. Watson. Collision theory. *(Wiley, New York)*, 1964.

[22] L. M. Delves. Tertiary and general-order collisions (ii). *Nucl. Phys.*, 20:275–308, 1960.

[23] M. Olshanii. Atomic scattering in the presence of an external confinement and a gas of impenetrable bosons. *Phys. Rev. Lett.*, 81:938–941, 1998.

[24] B. Paredes, A. Widera, V. Murg, O. Mandel, S. Folling, I. Cirac, G. V. Shlyapnikov, T. W. Hansch, and I. Bloch. Tonks-Girardeau gas of ultracold atoms in an optical lattice. *Nature*, 429:277–281, 2004.

[25] H. Feshbach. Unified theory of nuclear reactions. *Ann. Phys.*, 5:357–390, 1958.

[26] U. Fano. Effects of configuration interaction on intensities and phase shifts. *Phys. Rev. A*, 124:1866–1878, 1961.

[27] D. E. Manolopoulos. An improved log derivative method for inelastic scattering. *J. Chem. Phys.*, 85:6425–6429, 1986.

[28] J.-M. Launay and M. Le Dourneuf. Hyperspherical close-coupling calculation of integral cross sections for the reaction $H+H_2 \rightarrow H_2+h$. *Chem. Phys. Letters*, 163:178–187, 1989.

[29] R. T. Pack and G. A. Parker. Quantum reactive scattering in three dimensions using hyperspherical(aph) coordinates. theory. *J. Chem. Phys.*, 87:3888–3921, 1987.

[30] T. P. Grozdanov. Photodetachment of an electron bound by a zero-range potential in magnetic fields of arbitrary strength. *Phys. Rev. A*, 51:607–610, 1995.

[31] E. L. Bolda, E. Tiesinga, and P. S. Julienne. Effective-scattering-length model of ultracold atomic collisions and feshbach resonances in tight harmonic traps. *Phys. Rev. A*, 66:013403–1–7, 2002.

[32] J. I. Kim, V. S. Melezhik, and P. Schmelcher. Suppression of quantum scattering in strongly confined systems. *Phys. Rev. Lett.*, 97:193203–1–4, 2006.

[33] F. T. Smith. Lifetime matrix in collision theory. *Phys. Rep.*, 118:349–356, 1960.

[34] V. Aquilanti, S. Cavalli, A. Simoni, A. Aguilar, J. M. Lucas, and D. De Fazio. Lifetime of reactive scattering resonances: q-matrix analysis and angular momentum dependence for the $F+H_2$ reaction by the hyperquantization algorithm. *J. Chem. Phys.*, 121:11675–11690, 2004.

[35] A. Simoni, J-M. Launay, and P. Soldán. Feshbach resonances in ultracold atom-molecule collisions. *Phys. Rev. A*, 79:032701–1–6, 2009.

[36] T. Bergeman, M. G. Moore, and M. Olshanii. Atom-atom scattering under cylindrical harmonic confinement: Numerical and analytic studies of the confinement induced resonance. *Phys. Rev. Lett.*, 91:163201–1–4, 2003.

[37] C. W. Clark. Low-energy electron-atom scattering in a magnetic field. *Phys. Rev. A*, 28:83–90, 1983.

[38] R. G. Newton. Threshold properties of scattering and reaction cross sections. *Phys. Rep.*, 114:1611–1618, 1959.